National Renewable Energy Laboratory
A national laboratory of the U.S. Department of Energy
Office of Energy Efficiency & Renewable Energy
Innovation for Our Energy Future

Theoretical and Experimental Approaches to >50% Solar Cells

December 14, 2004 – March 13, 2008

C. Honsberg
University of Delaware
Newark, Delaware

Subcontract Report
NREL/SR-520-47655
May 2010

NREL is operated for DOE by the Alliance for Sustainable Energy, LLC Contract No. DE-AC36-08-GO28308

Theoretical and Experimental Approaches to >50% Solar Cells

December 14, 2004 – March 13, 2008

C. Honsberg
University of Delaware
Newark, Delaware

NREL Technical Monitor: Fannie Eddy

Prepared under Subcontract No. XAT-5-44277-01

Subcontract Report
NREL/SR-520-47655
May 2010

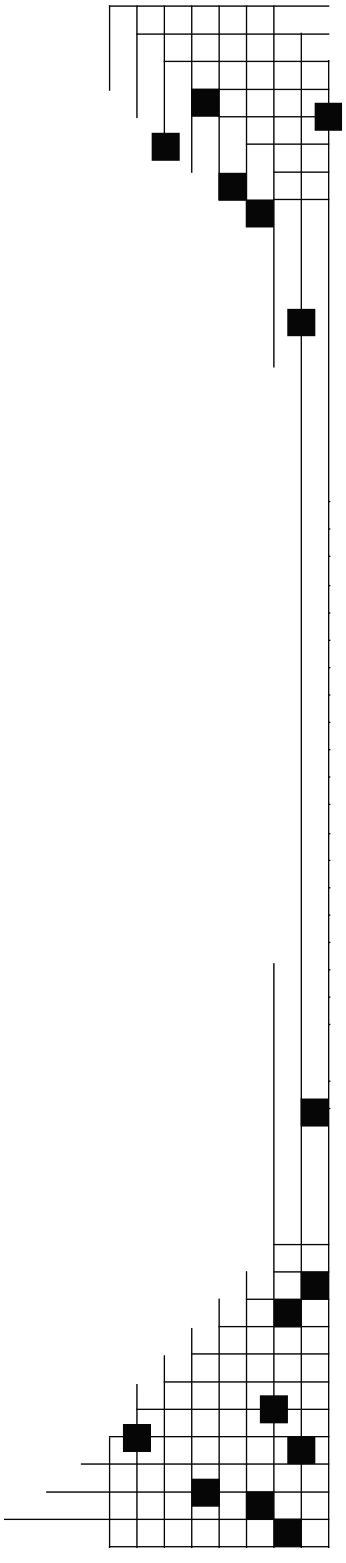

National Renewable Energy Laboratory
1617 Cole Boulevard, Golden, Colorado 80401-3393
303-275-3000 • www.nrel.gov

NREL is a national laboratory of the U.S. Department of Energy
Office of Energy Efficiency and Renewable Energy
Operated by the Alliance for Sustainable Energy, LLC

Contract No. DE-AC36-08-GO28308

Available electronically at http://www.osti.gov/bridge

Available for a processing fee to U.S. Department of Energy
and its contractors, in paper, from:
U.S. Department of Energy
Office of Scientific and Technical Information
P.O. Box 62
Oak Ridge, TN 37831-0062
phone: 865.576.8401
fax: 865.576.5728
email: mailto:reports@adonis.osti.gov

Available for sale to the public, in paper, from:
U.S. Department of Commerce
National Technical Information Service
5285 Port Royal Road
Springfield, VA 22161
phone: 800.553.6847
fax: 703.605.6900
email: orders@ntis.fedworld.gov
online ordering: http://www.ntis.gov/ordering.htm

This publication received minimal editorial review at NREL

Printed on paper containing at least 50% wastepaper, including 20% postconsumer waste

Summary

A central challenge in photovoltaics is to develop and implement approaches that allow photovoltaics to reach their thermodynamic efficiency limits. Tandem solar cells allow high efficiency, but as the number of solar cells in the tandem stack increases, they require increasing numbers of ideal, compatible materials and the incremental efficiency gains become smaller. An alternative approach is to develop solar cell structures based on previously unutilized physical mechanisms. The central goal of the project is to develop a physical understanding, design rules, materials, and device approaches to implement advanced concept photovoltaics, focusing particularly on multiple quasi-Fermi level or intermediate-band approaches. An overview of the accomplishments is given below.

- Demonstration that advanced concept approaches can be grouped in to one of five fundamental categories, and that the efficiency limits—and advantages and disadvantages— in each category are similar.
- Identification of fundamental loss mechanisms in multiple-energy-level solar cells.
- Design rules for intermediate-band materials and calculation of efficiency contour plots for multiple-level solar cells, indicating how sensitive the efficiencies are to changes in band-structure parameters.
- Thermodynamically and physically consistent model of the intermediate-band concept, including the effect of finite width of the band on the efficiency and the impact of absorption in the intermediate band, and calculation of absorption and emission rates.
- Calculation of the impact of finite intermediate-band width and absorption within the intermediate-band efficiency.
- Calculation and inclusion of non-ideal absorption coefficients for an intermediate-bandgap, spectral selectivity and impact of density of states on intermediate-band solar cell efficiency.
- Identification of materials used to implement multiple-energy-level solar cells which, based on ideal band structure, allow efficiencies of 50% at 1000x.
- Calculation of ideal intermediate-band solar cell bandgaps under AM1.5 and finite concentration.
- Epitaxial growth of the GaAsSb/GaAs system.
- Epitaxial growth of InAs quantum dots on GaAsSb.
- Observation of photoluminescence from the InAs quantum dots in GaAsSb.
- Inclusion of strain in InAs/GaAsSb band-structure modeling.

Thermodynamic grouping of advanced concept approaches. The large number of approaches and ways to implement advanced concept approaches can make comparison and analysis of solar cells based on such new concepts difficult. Despite the large number of approaches, from a thermodynamic standpoint, all advanced-concept approaches can be grouped according to which of the assumptions in thermodynamic modeling of conventional pn junctions it allows the solar cell to beneficially circumvent. The advantage of such a

grouping is that the design rules and losses are similar among approaches within a single class. The advanced-concept approaches and some implementations are shown in Table 1.

Table 1: Approaches to solar cells that exceed Shockley-Queisser limit for a single solar cell.

Approach	Advantages/Uses	Central Issues	Examples
Multiple spectrum	• Can be implemented using low-cost coatings • Can use existing solar cells (or light-emitting diodes [LEDs] for thermophotonics)	Efficient conversion of solar spectrum not demonstrated	Thermophotovoltaic Up and down conversion
Multiple absorption	• High impact-ionization rates demonstrated with colloidal quantum dots • Suited to conversion of high-energy photons	Transport of carriers not demonstrated	Multiple exciton generation Two-photon absorption Raman absorption
Multiple energy level	• Suited to low-energy photon conversion • Can capitalize on LED/photodetector devices	Need demonstration of multiple simultaneous radiative transitions of similar magnitude	Localized band (quantum well [QW]) Mini-band (intermediate-band solar cell)
Multiple temperate	Potential for high efficiencies using a single absorber material	Extraction of energy from hot-carrier populations not demonstrated	Hot carriers QWs with thermal escape
AC solar cells	Potential for high efficiencies using a single absorber material	Requires THz devices	Rectenna

Ideal band structure for intermediate-band solar cells. The ideal intermediate-band structure has bandgap values of 1.95, 1.2, and 0.7 eV for maximum concentration under a blackbody spectrum. In addition to these values, there are several other requirements for the band structure of an intermediate-band solar cell as shown in Figure 1a. These are that: (1) the valence-band offset is small; (2) there is only a single band or energy level between the conduction band and the energy levels formed by the overlap of quantum dots (QDs); and (3) the upper energy levels of the QD should not be within 3/2 kT of the continuum. Theoretically, the role of the valence band and conduction band may be switched, particularly if the hole effective mass is smaller than the electron effective mass. Condition (1) arises from the fact that the hole effective masses are typically larger than electron effective masses, and if there is a valence-band offset, the energy levels in the valence band of the QD will be closely spaced, allowing thermalization between the energy levels and leading to the inability to maintain a separate quasi-Fermi level in the QD valence band compared to the barrier valence band. This, in turn, means that an offset in the valence band gives a loss in open-circuit voltage (V_{OC}). Similar arguments also give conditions (2) and (3).

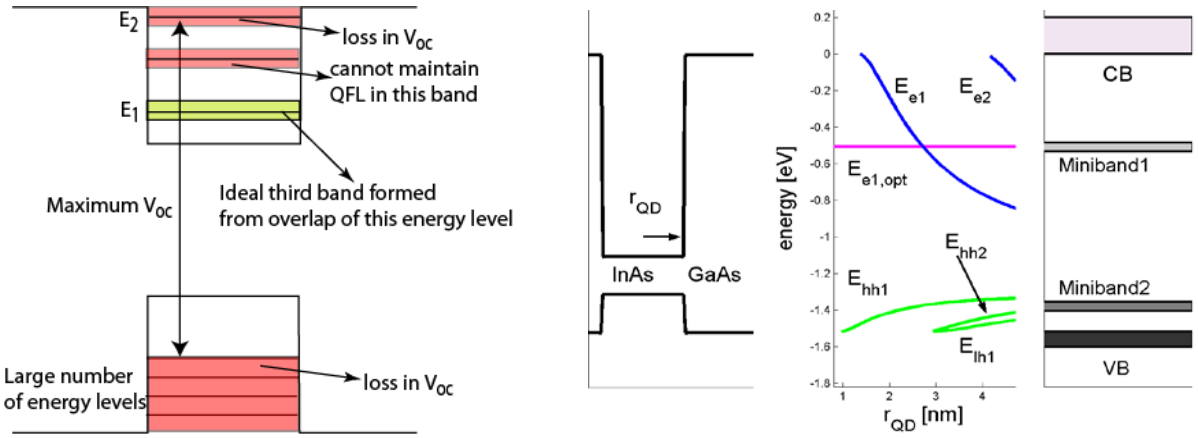

Figure 1: (a) Schematic of band structure, showing ideal intermediate-band (in green) and non-ideal band structure elements (in red). (b) Band structure (neglecting strain) for InAs QD in GaAs barrier, showing presence of non-idealities.

The additional requirements on band structure have a significant impact for materials for intermediate-band solar cells. For example, Figure 1b shows the band structure of an InAs QD (neglecting strain) with a GaAs barrier. Although the bandgaps are relatively close to their optimum values (and can be made ideal by replacing GaAs with AlGaAs), the band offsets and presence of additional bands means that such materials are not ideal.

Design rules for intermediate-band materials and calculation of efficiency contour plots for >60%. The bandgaps and other band-structure features for an ideal material give rise to a limiting set of conditions that make it difficult to find an ideal material. However, by relaxing the constraint from an ideal material to one for about >50% at 1,000 suns (rather than 63% at maximum concentration), there is substantial relaxation in the allowable materials. The design rules for a QD intermediate-band (IB) material are:

- Largest bandgap E_{CV} ranges from 1.40 to 2.56 eV.
- Single, narrow IB with bandgap, $E_{CI} = 0.5\ E_{CV} - 0.2$ eV.
- Fermi energy, EF, located near to (within) the IB.
- Substrate commercially available with lattice constant between QD's and barrier's.
- QD/barrier has minimum valence band offset.
- Lattice mismatch > 1% between barrier and QD material.

Efficiency contour plots provide a graphical way of examining the relationship between bandgaps and efficiency. Figure 2 shows efficiency contour plots for 1,000x, showing that >55% efficiency can be realized with a range of bandgaps.

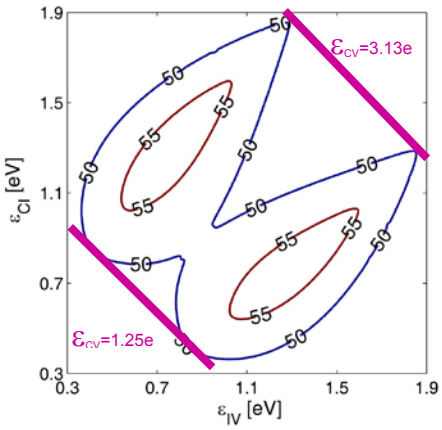

Figure 2: Efficiency contour plots for intermediate-band solar cell at 1,000x.

Thermodynamic formulation for inclusion of non-idealities. The conventional thermodynamic formulation for an intermediate-band solar cell is poorly suited to inclusion of non-idealities. Three changes were implemented to extend the type and range of non-idealities. These include the following: (1) inclusion of finite width of intermediate band and non-idealities associated with this band; (2) new mathematical formulation for Bose-Einstein equation, allowing calculations with greater precisions and more rapid calculations; (3) inclusion of extended band-structure model, allowing calculation of absorption and emission rates, absolute rather than relative position of the Fermi-levels, and effects such as non-ideal absorption.

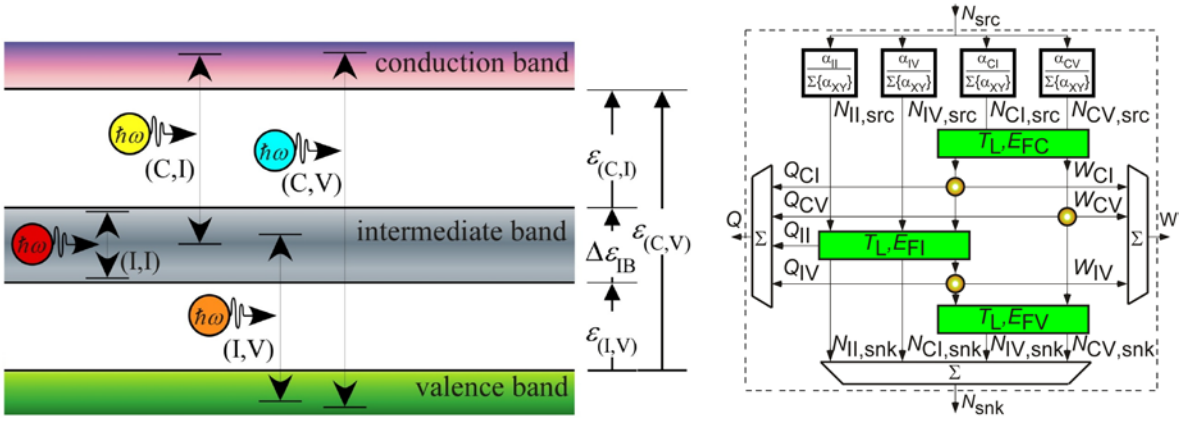

Figure 3: (a) Schematic band structure for an intermediate-band solar cell, showing absorption for each band. (b) Schematic of the thermodynamic formulation for the intermediate-band solar cell, showing losses in the intermediate band and non-ideal absorption coefficients.

Calculation of the impact of finite intermediate-band width and absorption within the intermediate band. The impact of a finite width of the intermediate-band solar cell efficiency and optimum bandgaps is shown in Figure 4 and Figure 5. Figure 4 shows the impact assuming that there is no absorption in the intermediate band and demonstrating the necessity of the expanded thermodynamic formulation that takes into account absorption losses in the intermediate band. For example, as the width of the intermediate band increases, the efficiency is reduced to that approximately of a two-junction tandem. In the case of an "infinite" width intermediate band, this leads to the condition in which the material should act like a blackbody, but calculations show that it has substantial efficiency. If the absorption within the intermediate band is included as shown in Figure 5, then, as expected, the

efficiency drops to zero as the intermediate band width increases. However, it is notable that until the bandwidth is over 1 eV, the degradation in efficiency is relatively small.

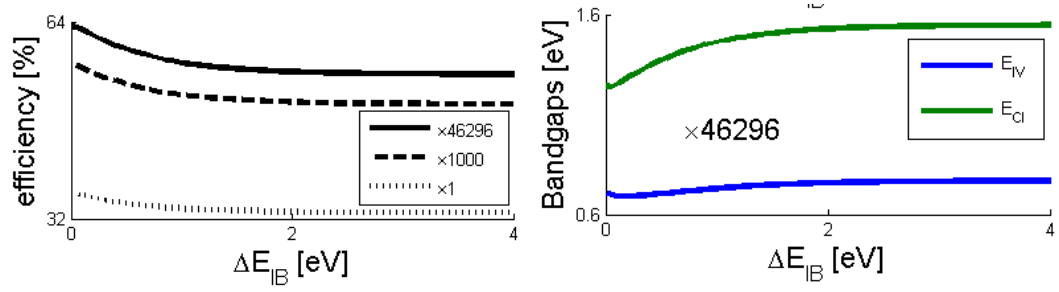

(a) (b)

Figure 4: (a) Efficiency as a function of intermediate band width for three different concentrations assuming that there is no absorption within the intermediate band. (b) Optimum values of the intermediate to conduction band energy and valence to intermediate band energy as a function of the intermediate band width.

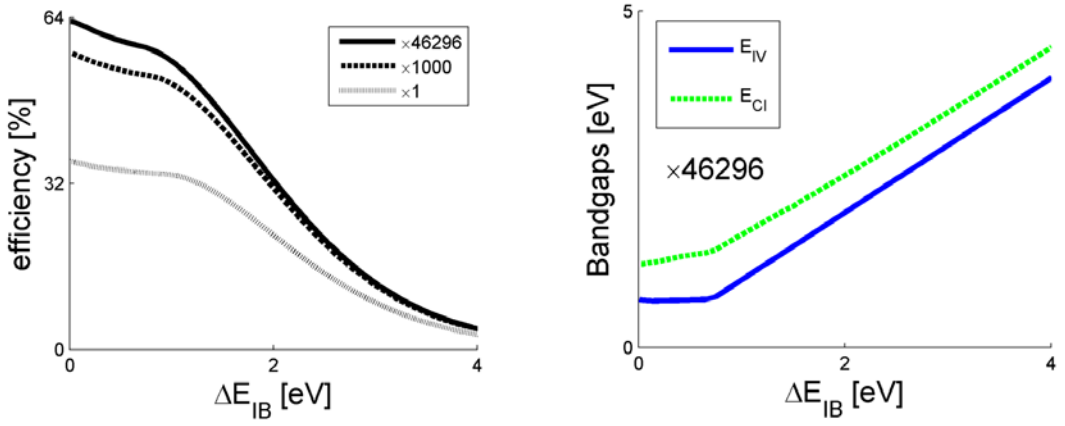

(a) (b)

Figure 5: (a) Efficiency as a function of intermediate band width for three different concentrations assuming absorption within the intermediate band. (b) Optimum values of the intermediate to conduction band energy and valence to intermediate band energy as a function of the intermediate band width.

Calculation and inclusion of non-ideal absorption coefficients for an intermediate bandgap and impact of density of states. A critical assumption in ideal intermediate band calculations is that of ideal absorption. Calculation of realistic absorption requires inclusion of an extended band diagram, including the density of states and transition matrix elements for the band structure. The assumed band structure is shown in Figure 6a. The band structure, with additional assumptions about parameters such as the effective masses needed to calculate the transition probabilities, allows calculation of the absorption coefficients. The ideal absorption coefficients are shown in Figure 6b, and Figure 7 shows absorption coefficients calculated for a range of density of states. Figure 7 shows the importance of the density of states in realizing ideal intermediate band absorbers.

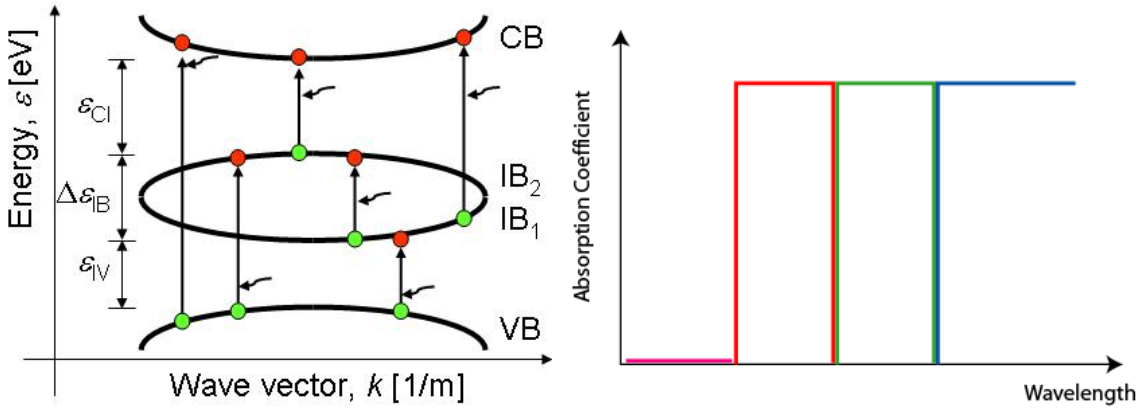

(a) (b)

Figure 6: (a) Assumed band structure for an intermediate-band material, showing parabolic band assumption. (b) Ideal absorption coefficients for an intermediate-band material.

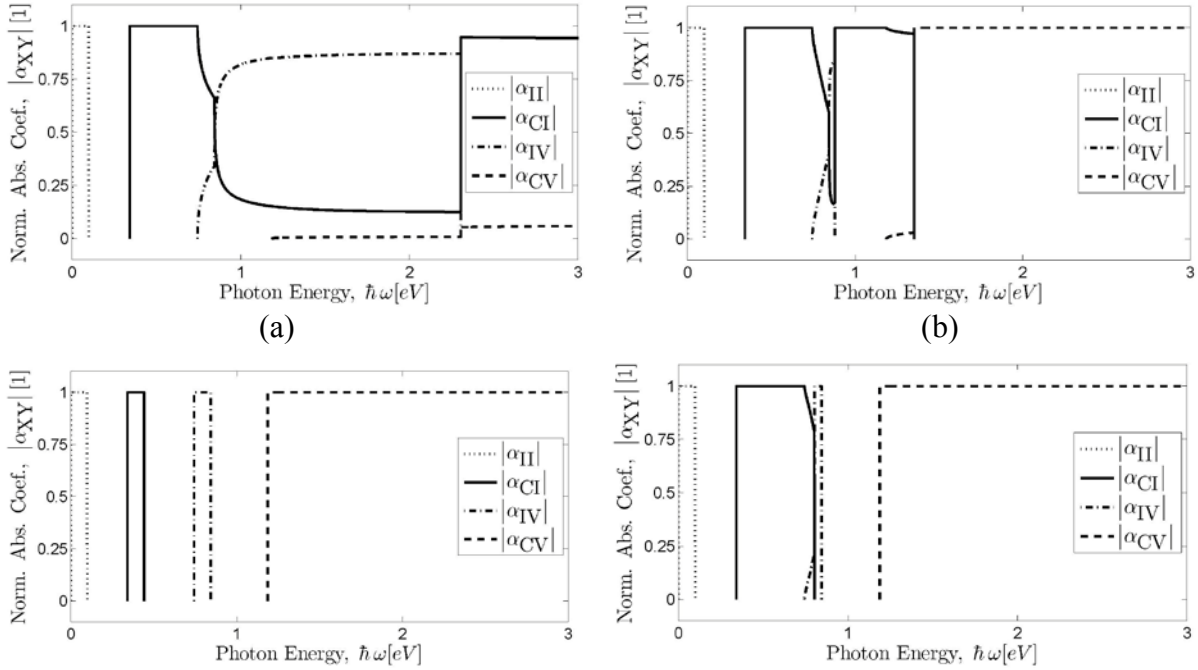

(a) (b) (c) (d)

Figure 7: Calculated absorption coefficients for: the intermediate band (α_{II}), the intermediate to conduction band (α_{CI}); the valence band to intermediate band (α_{IV}); and the valence to the conduction band (α_{CV}). Plots (a) to (d) differ in the assumed density of states, increasing from (a) to (d). Absorption coefficients are non-ideal in that they show: (a) overlap of absorption from different bands; (b) overlap of absorption from different bands; (c) incomplete absorption of the solar spectrum; and (d) incomplete absorption of the solar spectrum and overlap from different bands.

Candidate materials for intermediate-band solar cells. Based on the material design rules for intermediate-band solar cells determined above, a program to calculate the electronic states and band offsets for tertiary and binary combinations of III-V materials was used to determine candidate intermediate-band materials. To keep the computation time to a minimum and allow a search over the entire material space, effects such as strain are not included. The optimum material combinations are shown in Table 2.

Table 2: Potential material combinations for intermediate-band solar cells. The first and last rows have an efficiency of 48%, but are included as binary QDs, which are more practical than tertiary alloys. The other combinations have efficiency potential >50%.

Substrate	Barrier	QD	E_{CV}	$E_{\Delta CB}$
InP	$GaAs_{0.88}Sb_{0.12}$	InAs	1.18	0.83
InP	GaAs	$InP_{0.85}Sb_{0.15}$	1.42	0.49
InP	GaAs	$InAs_{0.40}P_{0.60}$	1.42	0.49
GaAs	$GaAs_{0.70}P_{0.30}$	InP	1.79	0.43

Calculation of bandgaps under AM1.5 and finite concentration. A critical constraint in the material selection for intermediate-band solar cells is the combination of a large conduction-band offset and a small (near zero) valence-band offset. This constraint can be relaxed to some degree by considering different concentrations and spectra. As in conventional tandems, an AM1.5 spectrum reduces the maximum bandgaps due to the lower number of high-energy photons. The optimum bandgaps for the intermediate-band solar cell is shown in Figure 8 for AM1.5 spectrum and 100x and 1,000x concentration. It shows that the difference between the global optimum intermediate bandgap and local optimum are relatively small, and further, that there is a larger range of optimum values.

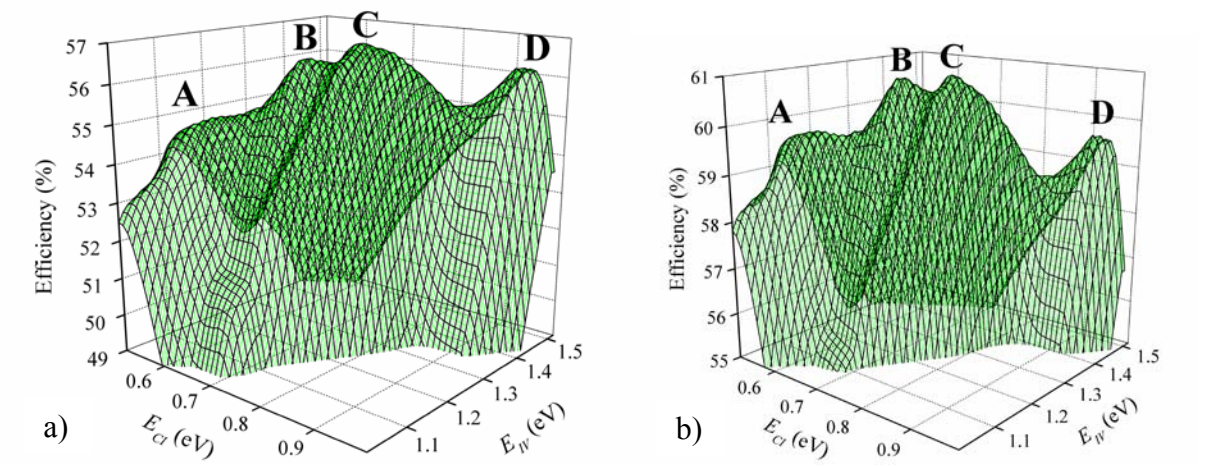

Figure 8: Optimum values of intermediate band to conduction band (E_{CI}) and valence band to intermediate band (E_{IV}) for AM.15 spectrum at (a) 100x and (b) 1,000x.

Epitaxial growth of the GaAsSb/GaAs system and growth of InAs QDs on GaAsSb. The GaAsSb material system has multiple advantages for an intermediate-band material. The bandgap ranges are close to ideal, offering the potential for high performance. In addition, depending on the material composition, there is a Type I to Type II transition when grown on GaAs, thus allowing a material in which the valence-band offset is zero. Further, Sb is reported to act as a surface passivator for InAs QDs, improving the optical properties of the QDs. Finally, Sb has other advantageous properties on QD properties, increasing the areal density of InAs QDs and assisting in aligning of QD chains. Despite these advantages, the growth of GaAsSb requires care because—unlike III-III-V ternaries where the composition is determined by the flux ratios of the Group III elements over a range of temperatures—in a III-V-V ternary, the composition also depends on the growth temperature. This becomes an issue

when growing QDs where the growth temperature of the barrier is typically different from that for the QD growth.

All of the samples studied were grown in an Applied Epi GenIII molecular beam epitaxy (MBE) system on semi-insulating GaAs (001) substrates. The Sb flux was provided by a Veeco all-PBN Corrosive Valved Cracker with the cracking zone held at 1000°C to ensure a Sb_2-rich flux. A Veeco Valved Cracker was used to provide the As flux with the cracking zone held at 950°C to ensure an As_2-rich flux. De-oxidation of the substrate surface under an As_2 flux was observed at ~580°C as measured by an IRCON infrared pyrometer.

Figure 9 summarizes the results. Two features become apparent regarding the dependence of the Sb content on the growth temperature and Sb flux. Firstly, as the temperature is increased, the Sb content decreases in a fairly linear manner in this range. This behavior fits with previous reports for high Sb content growth of GaAsSb where increased temperature saw the As content drop [1]. This behavior has been attributed to a As/Sb exchange reaction that increases with increased temperature [2]. Secondly, as expected, the Sb content increases with higher Sb flux, but it appears to be a non-linear dependence. This confirms previous results reported by Wu et al. [3], where the Sb was found to be very sensitive to changes in Sb flux for low Sb flux and content while being less sensitive for higher fluxes and contents. These results agree with predictions made by non-equilibrium thermodynamic analysis of III-V-V compounds [4]. Further, as shown in Figure 9b, reciprocal space maps show that the defect density is low.

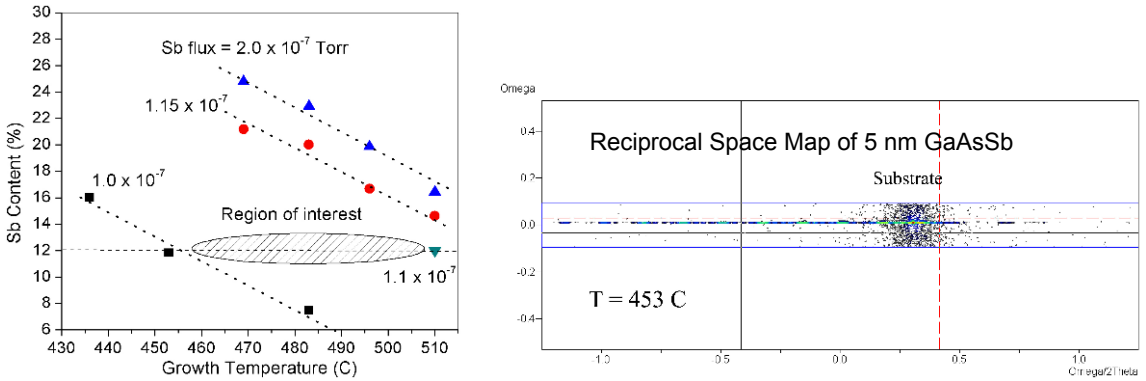

Figure 9: (a) Sb content in GaAsSb as a function of the growth temperature and the Sb flux. The growth rate for all of the samples was ~0.40 monolayers/s. The dotted lines are guides to the eye only. (b) Reciprocal space maps obtained for two samples of ~12% Sb composition grown at T = 453°C.

<u>Epitaxial growth of InAs quantum dots on GaAsSb.</u> The addition of Sb changes the formation of InAs QDs compared to growing them on GaAs, both because Sb may act as a surfactant and also because the Sb composition changes the strain associated with the self-assembly of the QDs. Figure 10 shows an example of the QD grown on GaAs compared to GaAsSb, showing the improved performance of the QDs grown on GaAsSb.

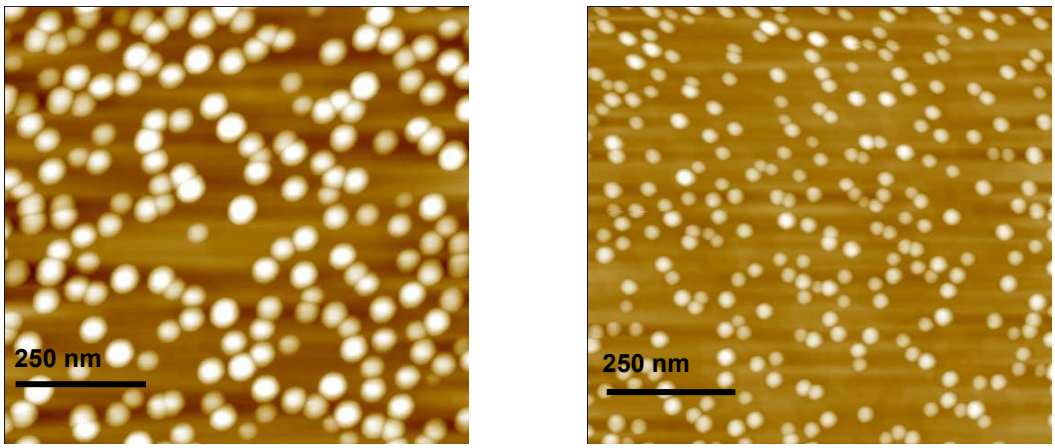

(a) (b)

Figure 10: (a) InAs QD on GaAs; (b) InAs QDs on GaAs (5 monolayers) / $GaAs_{1-x}Sb_x$ (5nm) buffer layers with x =23%, with density 2.6 x 10^6 cm^{-2}

Measurement and modeling of photoluminescence from InAs QDs on GaAsSb. To be an effective intermediate-band material, the three energy levels in an intermediate-band solar cell must be radiatively coupled. Consequently, it is essential that the QD system has radiative emission. As a first step in demonstrating radiative emission between all three energy levels, there should be a radiative signature. Through collaboration with Prof. Stoleru in Material Science and Engineering at the University of Delaware, time-resolved photoluminescence was measured on InAs QD samples and samples without QDs. The results are shown in Figure 11, with the expected band diagram shown in Figure 11b (not to scale). The results show a shift in the radiative signal with the InAs QDs, and results are consistent with the expected band diagram, showing a radiative transition of 1.1 eV and a calculated conduction-band offset of about 300 mV.

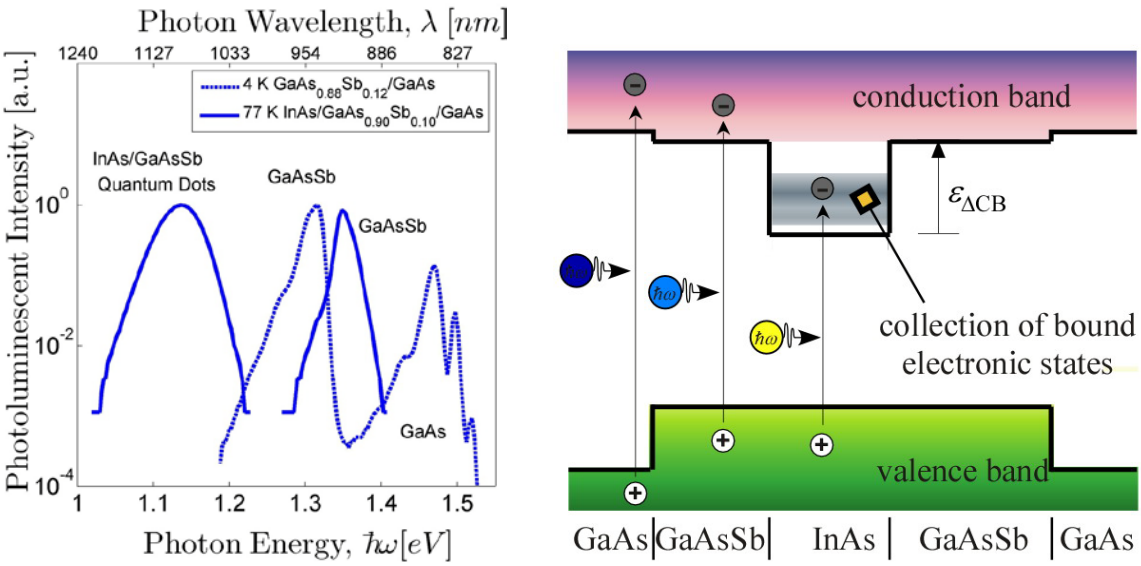

Figure 11: (a) Photoluminescence spectra of a InAs QD with a layer structure as shown in (b) and a GaAs/GaAsSb structure.

Strain calculations for InAs QDs on GaAsSb material. To accurately determine the band structure of the QD material, strain must be incorporated into the band-structure calculations. To calculate a more accurate band structure for InAs QDs on GaAsSb, k·p modeling for the

band structure was combined with strain models for pyramidal QDs. Figure 12 shows the strain calculations in a pyramidal QD. The impact of the strain on band structure was calculated using k·p modeling approaches. For an InAs QD on InPSb, the band structure is shown in Figure 13. For the compressive strain encountered in III-V materials, the conduction-band offset tends to decrease, degrading the efficiency potential of the intermediate-band approach. To compensate for this effect, the unstrained conduction-band offset should be increased; however, materials with such large conduction-band offsets and no valence-band offset are not common in the III-V material system. However, the expanded design space of the AM1.5G spectrum and variable concentration increases the flexibility in material choices, and the Sb-based material system with InAs QD allows relatively ideal intermediate-band materials, retaining over 90% of the theoretical maximum efficiency.

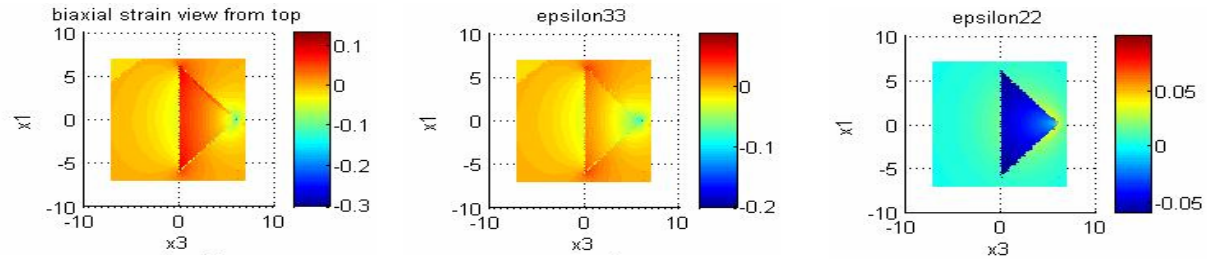

Figure 12: Strain in a pyramidal InAs QD, showing the biaxial and hydrostatic strain in the QD.

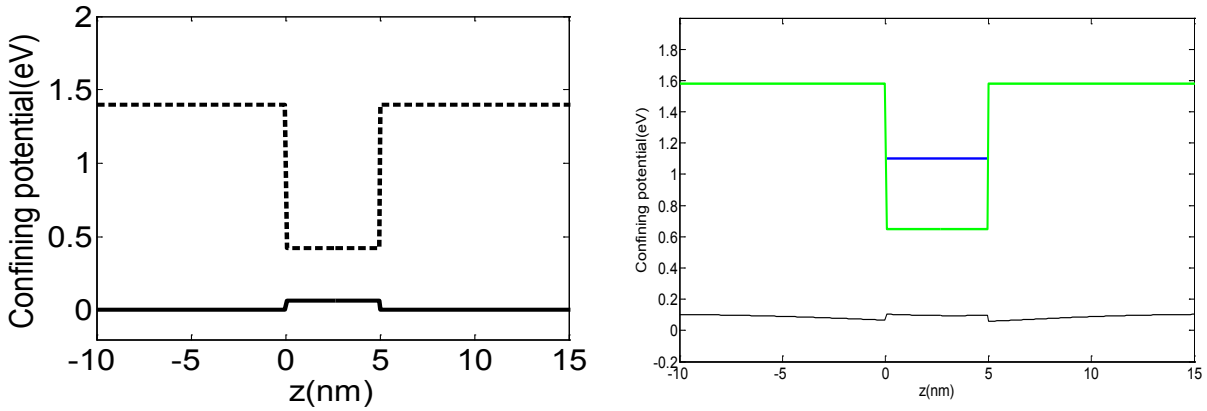

Figure 13: Band structure for a pyramidal InAs QD on InPSb (a) neglecting strain and (b) including the strain profile.

References

1. E. Selvig, B.O. Fimland, T. Skauli, and R. Haakenaasen, *Journal of Crystal Growth* **227-228**, p562, 2001.
2. Q. Xie, J.E. Van Nostrand, J.L. Brown, and C.E. Stutz, *Journal of Applied Physics* **86**, p329, 1999.
3. S.D. Wu, L.W. Guo, W.X. Wang, Z.H. Li, X.Z. Shang, H.Y. Hu, Q. Huang, and J.M. Zhou, *Journal of Crystal Growth* **270**, p359, 2004.
4. A. Yu. Egorov, A.R. Kvosh, V.M. Ustinov, A.E. Zhukov, P.S. Kop'ev, and C.W. Tu, *Journal of Crystal Growth* **188**, p69, 1998.

REPORT DOCUMENTATION PAGE

Form Approved
OMB No. 0704-0188

PLEASE DO NOT RETURN YOUR FORM TO THE ABOVE ORGANIZATION.

1. REPORT DATE *(DD-MM-YYYY)*	2. REPORT TYPE	3. DATES COVERED *(From - To)*
May 2010	Subcontract Report	12/14/04 - 03/13/08

4. TITLE AND SUBTITLE
Theoretical and Experimental Approaches To >50% Solar Cells

5a. CONTRACT NUMBER
DE-AC36-08-GO28308

5b. GRANT NUMBER

5c. PROGRAM ELEMENT NUMBER

6. AUTHOR(S)
C. Honsberg

5d. PROJECT NUMBER
NREL/SR-520-47655

5e. TASK NUMBER
PVA7.2001

5f. WORK UNIT NUMBER

7. PERFORMING ORGANIZATION NAME(S) AND ADDRESS(ES)
University of Delaware
Electrical and Computer Engineering
Newark, DE 19716

8. PERFORMING ORGANIZATION REPORT NUMBER
XAT-5-44277-01

9. SPONSORING/MONITORING AGENCY NAME(S) AND ADDRESS(ES)
National Renewable Energy Laboratory
1617 Cole Blvd.
Golden, CO 80401-3393

10. SPONSOR/MONITOR'S ACRONYM(S)
NREL

11. SPONSORING/MONITORING AGENCY REPORT NUMBER
NREL/SR-520-47655

12. DISTRIBUTION AVAILABILITY STATEMENT
National Technical Information Service
U.S. Department of Commerce
5285 Port Royal Road
Springfield, VA 22161

13. SUPPLEMENTARY NOTES
NREL Technical Monitor: Fannie Eddy

14. ABSTRACT *(Maximum 200 Words)*
A central challenge in photovoltaics is to develop and implement approaches that allow photovoltaics to reach their thermodynamic efficiency limits. Tandem solar cells allow high efficiency; but as the number of solar cells in the tandem stack increases, they require increasing numbers of ideal, compatible materials and the incremental efficiency gains become smaller. An alternative approach is to develop solar cell structures based on previously unutilized physical mechanisms. The central goal of the University of Delaware's project is to develop the physical understanding, design rules, materials, and device approaches to implement advanced concept photovoltaics, focusing particularly on multiple quasi-Fermi level or intermediate-band approaches.

15. SUBJECT TERMS
PV; very high efficiency; thermodynamic efficiency limits; advanced concepts; multiple quasi-Fermi level approach; intermediate-band approach

16. SECURITY CLASSIFICATION OF:			17. LIMITATION OF ABSTRACT	18. NUMBER OF PAGES	19a. NAME OF RESPONSIBLE PERSON
a. REPORT	b. ABSTRACT	c. THIS PAGE			
Unclassified	Unclassified	Unclassified	UL		19b. TELEPHONE NUMBER (*Include area code*)

Standard Form 298 (Rev. 8/98)
Prescribed by ANSI Std. Z39.18